ACS APPLIED MATERIALS & INTERFACES

Research Article

www.acsami.org

Enhanced Charge-Carrier Transport through Shorter Carbon Nanotubes in Organic Photovoltaics

Xinbo C Lau, Zheqiong Wu, and Somenath Mitra*

Department of Chemistry and Environmental Science, New Jersey Institute of Technology, Newark, New Jersey 07102, United States

ABSTRACT: We demonstrate for the first time the efficiency improvement of organic photovoltaics by the addition of shorter multiwalled carbon nanotubes (MWNTs) generated by size sorting. The different size MWNTs were generated by size sorting a batch of carboxylated MWNTs and were introduced as charge carriers in poly(3-hexylthiophene) (P3HT):phenyl-C61-butyric acid methyl ester (PCBM) bulk heterojunction photovoltaic cells. As compared to a control with only PCBM, the addition of the long and short MWNT resulted in 12 and 34% improvement in short circuit current density (J_{sc}) respectively. The results indicate that length of carbon nanotubes is an important consideration in photovoltaic and possibly other nanoelectronic devices.

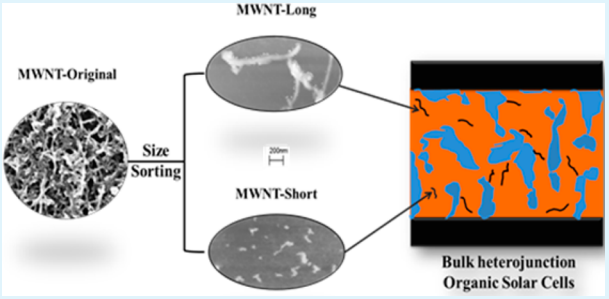

KEYWORDS: *short carbon nanotubes, size sorting, OPV, PCBM, CNT, P3HT*

1. INTRODUCTION

Organic photovoltaics (OPVs) are a promising low-cost alternative to silicon solar cells, particularly because they can be made via coating processes to cover large areas, and may be fabricated on flexible plastic substrates.[1−4] Devices incorporating conjugated polymers were enabled by the discovery of photoinduced charge transfer from polymers to Fullerene (C_{60}) and its derivatives such as phenyl-C61-butyric acid methyl ester (PCBM). In spite of relatively high open circuit voltages (V_{OC}), bulk heterojunction OPVs suffer from low power conversion efficiency (PCE) because they tend to have low short circuit current density (J_{SC}). Achievement of better charge carrier transport could be a path to higher PCE. Moreover, in a heterojunction structure, the charge carriers encounter their opposite carriers during transport, leading to charge carrier recombination.[5,6] Therefore, efficient charge-carrier transport and optimization of conditions for their facilitation is of great importance for the future development of OPVs.

It is well-known that OPVs performance is strongly dependent on the nanoscale morphology of the active layer, the phase separation between donors and acceptors and the formation of interconnected percolation networks. It has been reported that carrier mobility can be improved by ameliorating the nanoscale morphology through introduction of nanomaterials.[7,8] Carbon nanotubes (CNTs) have been successfully added to the OPVs composite to act as charge carriers/transporters.[9−15] This has been accomplished by blending into OPVs matrix[16,17] or compositing CNTs with fullerenes.[11,18] Although the CNTs have been also used as charge separators, their high electron and hole mobilities on the order of 1×10^8 cm^2/Vs and 1×10^3 cm^2/Vs, respectively. It has been found to enhance PCE.[11,17,19,20] However, the gains in PCE have been modest because of the relatively long lengths of the CNTs, which can cause a short circuit as well as be sites for charge recombination.[16] The CNTs are expected to act as electron-transporting pathways as well as electron acceptors[10,21−23] and the CNTs may also provide a larger surface area at the donor−acceptor (D/A) interface for more efficient exciton dissociation.[24−26] Other interesting approaches include integration of functionalized single-walled CNTs in P3HT:PCBM to enhance PCE from 1 to 1.4%,[27] covalent modification of single-walled CNTs by thiophene to improve PCE from 1 to 1.78% based on P3HT:PCBM,[16] and N-doped MWNTs has been reported to facilitate charge separation and transport from 7.3 to 8.6% based on OPVs made from PTB7:PC71BM.[28]

Precise control of size and morphology of additives is needed before they can be implemented into an OPV structure. Typical CNTs are a heterogeneous mixture of different lengths. The long CNTs tend to be more tangled and provide a tortuous path for electron transport,[29,30] and may lead to more short circuit and charge recombination. Shorter CNTs could improve dispersibility as well as charge-transport properties.[29] It's possible that this problem alleviated using shorter CNTs and one with less heterogeneity. The latter could lead to a more defined architecture. The shorter CNTs may also provide a larger surface area at the donor and acceptor interface, which would be favorable for efficient dissociation of excitons. Recent developments in size sorting by high-speed centrifugation, field-flow fractionation, gel electrophoresis, capillary electrophoresis, and size-exclusion chromatography and high performance liquid chromatography make it a viable possibility.[30] The objective of this research was to study the implementation of

Received: October 16, 2013
Accepted: January 10, 2014
Published: January 10, 2014

   dx.doi.org/10.1021/am404543r | ACS Appl. Mater. Interfaces 2014, 6, 1640−1645

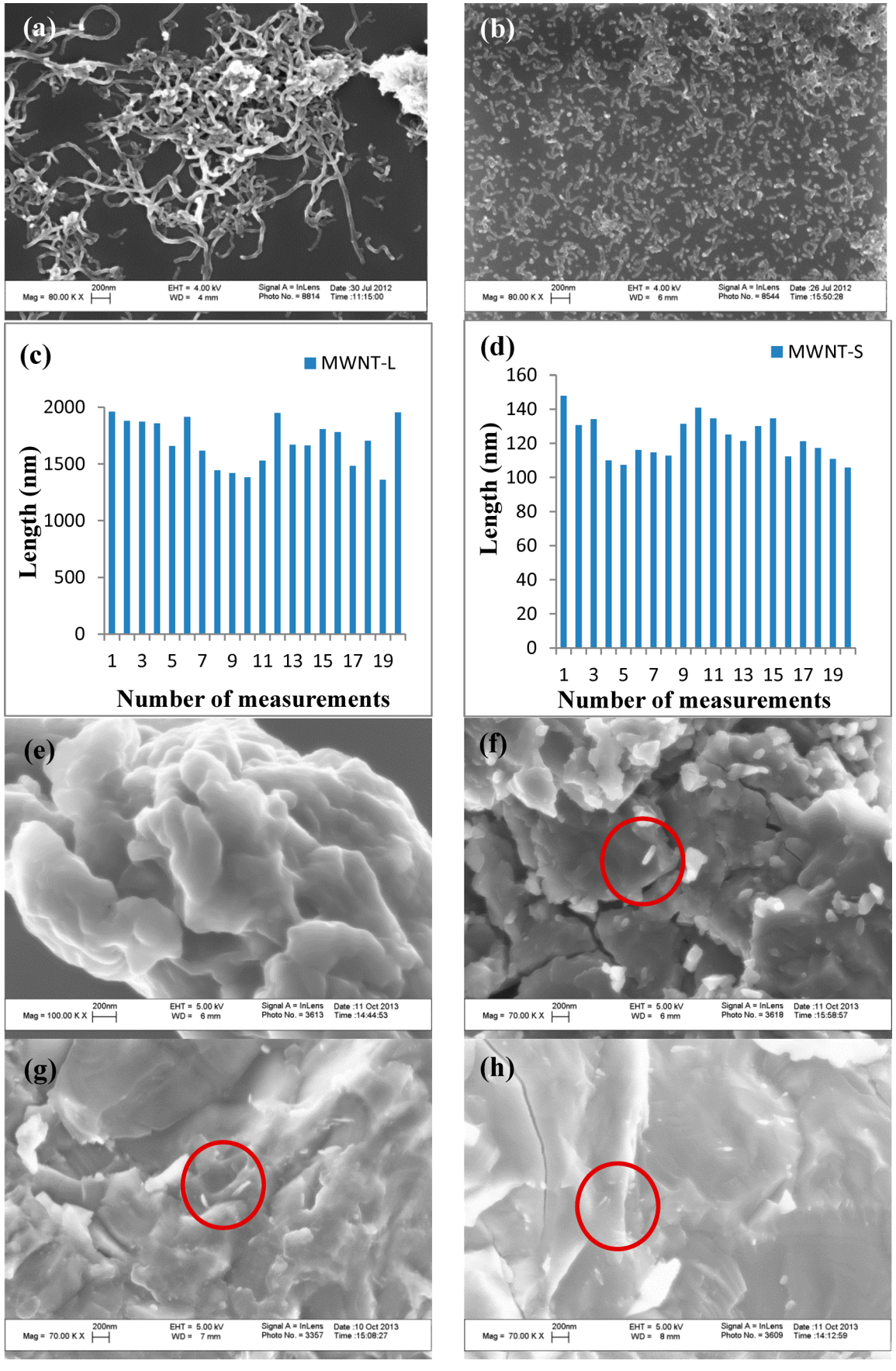

Figure 1. SEM images of (a) MWNT-L, (b) MWNT-S, (c) length measurement of MWNT-L, (d) MWNT-S, (e) P3HT:PCBM, (f) P3HT:PCBM-MWNT-O, (g) P3HT:PCBM- MWNT-L, and (h) P3HT:PCBM-MWNT-S.

dx.doi.org/10.1021/am404543r | *ACS Appl. Mater. Interfaces* 2014, 6, 1640−1645

Table 1. Photovoltaic Parameters under 95 mW/cm^2 Simulated Solar Irradiation Measured after Thermal Annealing at 125 °C

photoactive layer	length (nm)	V_{oc} (V)	current density (mA cm^{-2})	fill factor (FF) (%)	PCE (%)
P3HT: PCBM		0.54 ± 0.01	4.77 ± 0.17	0.44 ± 0.02	1.20 ± 0.06
P3HT: PCBM with MWNT-O	500−2000	0.54 ± 0.01	5.2 ± 0.11	0.46 ± 0.01	1.35 ± 0.04
P3HT: PCBM with MWNT-L	1695 ± 204	0.51 ± 0.03	5.35 ± 0.36	0.45 ± 0.01	1.33 ± 0.09
P3HT: PCBM with MWNT-S	123 ± 12	0.53 ± 0.03	6.39 ± 0.5	0.44 ± 0.04	1.56 ± 0.12

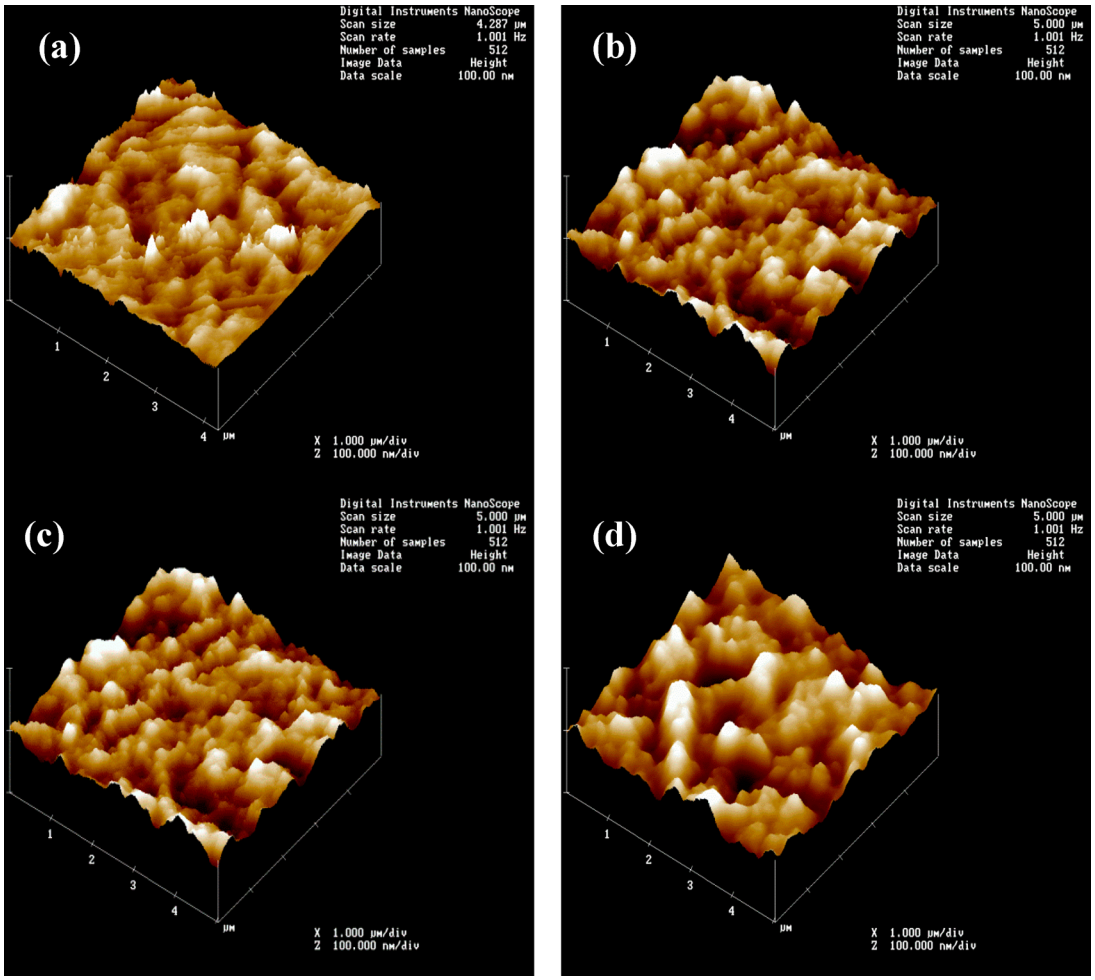

Figure 2. AFM images of active layers of (a) P3HT:PCBM, (b) P3HT:PCBM-MWNT-O, (c) P3HT:PCBM-MWNT-L, and (d) P3HT:PCBM-MWNT-S.

MWNTs of different lengths in conventional P3HT:PCBM solar cell for enhanced charge transport. To eliminate the effect of variables such as batch-to-batch variation and pretreatment, CNTs of different lengths that were size segregated from the same batch were incorporated into the active layer to study the effect of length.

2. EXPERIMENTAL SECTION

2.1. Preparation and Size Segregation of MWNTs. The synthesis of the carboxylated multi-walled carbon nanotubes were carried out under the Microwave Accelerated Reaction System. Pre-weighed MWNTs (from Cheap tubes Inc. with the length of 500−2000 nm and diameter of 30−50 nm) were added to reaction chamber together with a mixture of concentrated H_2SO_4 and HNO_3. The reaction vessels were subject to microwave radiation at a preset temperature of 140 °C for 20 min. After being cooled to room temperature, the product was vacuum filtered using Milli-Q water with pore size 10 μm, until the filtration reached a neutral pH. The carboxylated MWNTs (MWNT-O) were dried in a vacuum oven at 70 °C until constant weight.

The long and short MWNTs were prepared from the same sample, thus eliminating the possibility of batch-to-batch variation was achieved. The original mixture was size sorted as follows. The highly dispersible MWNT-O was sonicated at low power to disperse in water and centrifuged at 10 000 rpm. The sediment was redispersed in water by sonication and centrifuged once again. The sediment represented the fraction with the longest CNTs and was used for fabricating OPVs. The solution phase from the first centrifugation at 10 000 rpm was sequentially centrifuged at 12 000, 14 000, and 16 000 rpm with the sediment being rejected at each step. The final suspension represented the fraction with the shortest length and was used to fabricate OPVs. The mean length of the long (MWNT-L) and short (MWNT-S) nanotube fractions were 1695 ± 204 nm and 123 ± 12 nm respectively. The concentrations of MWNT-L and MWNT-S were quantified by a HP 845 UV−visible absorption spectrophotometer. The desired optimum concentration of 0.01 mg/mL was obtained via dilution. MWNT-O, MWNT-L, and MWNT-S solutions were sonicated at low power to achieve good dispersions without damaging

the MWNTs. Morphology of the MWNTs was studied by using a LEO 1530 VP field-emission scanning electron microscope (SEM).

2.2. Solar Cell Fabrication and Characterization. The bulk heterojunction OPVs were fabricated as follows. PCBM powder with a purity of 99.98% was obtained from MER Corporation, and orthodichlorobenzene (ODCB) was obtained from Fisher Scientific. Regioregular P3HT was obtained from Reike Metals Inc. Bulk PCBM solution in ODCB was prepared at a concentration of 10 mg/mL, 0.3ml of the MWNT-O solution at a concentration of 0.1 mg/mL was added into 3ml of PCBM solution and sonicated for 10 min. MWNT-L and MWNT-S solutions with PCBM solution were prepared in the same method. The suspension was then mixed with fifty weight percent of P3HT and stirred overnight at room temperature. All three compositions (active layer composite solutions) formed uniform and stable dispersions in ODCB, similar process has been reported previously.[19] A similar 1:1 solution of P3HT and PCBM (active layer solution) was also prepared by dissolving directly the two components in ODCB and stirring overnight. OPVs were fabricated onto indium–tin-oxide (ITO) coated glass. These were patterned prior to being cleaned with detergent, rinsed with DI water and washed with acetone and isopropanol. They were dried with compressed nitrogen and put inside the oven for 5 min at 110°C. Aqueous dispersion of Poly(ethylenedioxy)-thiophene:poly(styrene)sulfonate (PEDOT:PSS) (conductive grade) was filtered and spin coated onto the cleaned glass substrates at 2800 rpm for 50 s. The samples were then dried inside the oven at one atmosphere at 110 °C for 30 min. This was spin-coated outside a glove box on top of the PEDOT:PSS buffer layer to produce a film with a thickness of around 100 nm at 470 rpm for 15 s and then at 780 rpm for 5 s. Then the sample was allowed to dry slowly in the sealed petri dish at room temperature. Finally, a 145 nm thickness of Aluminum (Al) cathode layer was deposited by thermal evaporation using a shadow mask at 7×10^{-7} Torr. The fabricated samples were annealed on hot plates at 125 °C for 10 min in a nitrogen glove box. The active cell area was around 0.272 cm^2 and was defined by the intersection of Al and ITO layers. Thin films of P3HT:PCBM, P3HT:PCBM-MWNT-O, P3HT:PCBM-MWNT-L, and P3HT:PCBM-MWNT-S were deposited on cleaned glass substrates by the same process. These were characterized by UV-visible absorption spectroscopy and atomic force microscopy AFM (Digital Instrument, NanoscopeII). SEM images were taken on thin films of the active layer solution and three active layer composite solutions prepared on cleaned Si wafers under same conditions. Photoluminescence spectra were studied by an F-7000 fluorescence spectrophotometer.

A Keithley 2400 source-measuring unit was used to measure current–voltage characteristics in the dark and under simulated solar irradiation. Newport 122W solar simulator with an AM 1.5G filter simulated radiation at 95 mW cm^{-2}. A calibrated thermopile detector (Thorlabs model S210A) was used to check the irradiation intensity before every measurement.

3. RESULTS AND DISCUSSION

3.1. Morphology of Different Sizes of MWNTs and Active Layers. SEM measurements were carried out to analyze size distributions of MWNT-L and MWNT-S, shown in Figure 1a–d and Table 1.[31] The mean length of MWNT-L was found to be 1695 ± 204 nm and the mean length of MWNT-S was 123 ± 12 nm. This clearly showed that there was a significant difference between two fractions.

The morphology of active layers of P3HT:PCBM with MWNT-O, MWNT-L, and MWNT-S was studied by SEM. It was seen that the implemetation of MWNTs altered the morphology of the films, and a few nanotubes could be seen on the film surfaces. AFM images of photovoltaic layer of P3HT:PCBM with MWNT-O, MWNT-L, and MWNT-S after annealing are shown in Figure 2. The morpholgy of the active layers was altered in the presence of different MWNTs. The surface roughness of P3HT:PCBM, P3HT:PCBM with MWNT-O, MWNT-L, and MWNT-S were 6.83 ± 0.41, 9.14 ± 0.22, 8.02 ± 0.15, and 10.9 ± 0.15 nm, resepctively. The surface roughness may lead to advantages such as larger domains, larger donor–acceptor interfaces and an increase in contact area which may affect the efficiency of charge collection at the electrode–polymer interface. It is also known to enhance internal reflection and light collection.[32] The introduction of MWNT-S increased the surface roughness of the active layer and also altered the texture into a much coarser film with broad hill-like features compared to the other films. As presented below, the devices with higher surface roughness showed superior device performance.

The UV spectra of P3HT:PCBM, P3HT:PCBM-MWNT-O, P3HT:PCBM-MWNT-L, and P3HT:PCBM-MWNT-S coated films are shown in Figure 3a. The introduction of different

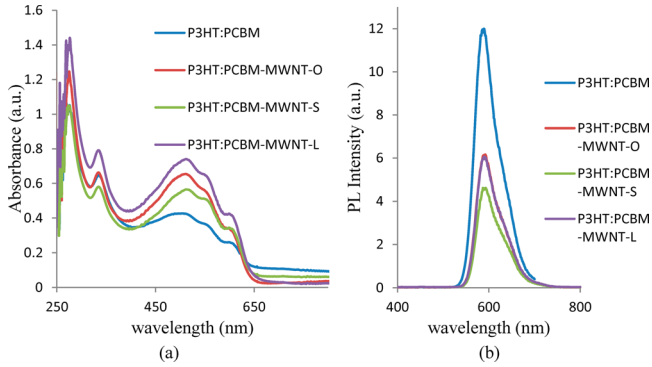

Figure 3. (a) UV absorption spectra and (b) PL spectra of P3HT:PCBM, P3HT:PCBM-MWNT-O, P3HT:PCBM-MWNT-L, and P3HT:PCBM-MWNT-S.

lengths of MWNT into P3HT:PCBM blend increased the absorption, which was in line with what has been published before,[31] and MWNT-L showed maximum enhancement. The PL spectra of P3HT:PCBM, P3HT:PCBM-MWNT-O, P3HT:PCBM-MWNT-L, and P3HT:PCBM-MWNT-S in ODCB are shown in Figure 3b. The strong PL peak at 587 nm is the signature for P3HT in ODCB. The observed PL for P3HT:PCBM blends indicates that some of the excitons generated in P3HT recombined. The addition of MWNT-O and MWNT-L to P3HT:PCBM blend reduced the PL intensity almost equally; however, implementation of MWNT-S quenched the intensity the most, from 11.4 to 4.8, which could imply that the implementation of MWNT-S contributes to the more efficient charge separation and resulted in the enhanced photocurrent density.[24]

3.2. Performance of Solar Cell Devices. *J–V* curves of different devices are shown in Figure 4 A and B and their performances (mean and standard deviation) are presented in Table 1. The data represents an average of eight measurements. On the basis of the student t-test, the difference in PCE among the different OPVs was significant at 95% confidence level. It is seen from Table 1 that although open circuit voltage and fill factor stayed the almost the same, short circuit current increase from 4.77 ± 0.17 to 5.2 ± 0.11, 5.35 ± 0.36, and 6.39 ± 0.5 mA cm^{-2} for P3HT:PCBM to that with MWNT-O, MWNT-L, and MWNT-S, respectively. The observed enhancement in the photocurrent was attributed to a more efficient charge carrier transport through the nanotube percolation pathways. Although single-walled CNTs have been used in P3HT:PCBM,[27] the photogenerated excitons are dissociated

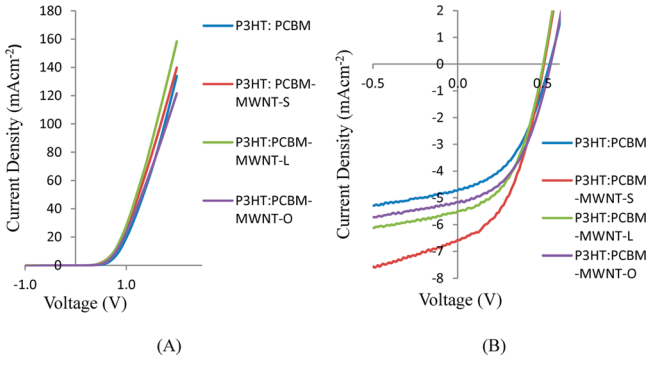

Figure 4. (A) $J-V$ characteristics in the dark of OPVs with (a) P3HT:PCBM, (b) P3HT:PCBM-MWNT-O, (c) P3HT:PCBM-MWNT-L, (d) P3HT:PCBM-MWNT-S. All of the cells were annealed at 125 °C for 10 min. (B) $J-V$ characteristics under simulated solar irradiation at 95 mW cm^{-2} for OPVs with (a) P3HT:PCBM, (b) P3HT: PCBM-MWNT-O, (c) P3HT:PCBM-MWNT-L, (d)- P3HT:PCBM- MWNT-S. All of the cells were annealed at 125 °C for 10 min.

at the P3HT:PCBM interfaces, and the electrons are transported to the respective electrode Al by hopping between the fullerene molecules. The integration of the nanotubes in the photoactive layer provides additional pathways for the electrons travelling through the dispersed carbon nanotube percolation network, suppressing charge recombination and enhancing electron transport.[27,29] The incorporation of MWNTs to P3HT:PCBM led to higher J_{sc}, which eventually led to more efficient electron transport. Therefore, PCE increased from 1.20 ± 0.06 for P3HT:PCBM to 1.35 ± 0.04, 1.33 ± 0.09, and 1.56 ± 0.12% for OPVs with MWNT-O, MWNT-L, and MWNT-S, respectively. The introduction of all three different lengths of MWNTs increased the efficiency of the devices and MWNT-S was the most effective one.

The introduction of MWNTs provided better percolation pathways for faster charge transport. The MWNT-S appeared to serve as better charge transport carriers than MWNT-L. With thickness of the active layer around 100 nm, the MWNT-S with mean length of 123 nm provided better and faster percolation for charge transport. On the other hand, the 1695 nm mean length of MWNT-O could increase the possibilities of short circuit and charge recombinition.

4. CONCLUSIONS

In conclusion, we demonstrated that short MWNTs are more effective charge carrier transporters in OPVs, and this led to the enhancement in power conversion efficiency by 30%. The introduction of MWNT enhanced short circuit current. The enhancement in J_{sc} for the original, long, and short MWNTs were 9, 12, and 34%, respectively. This improvement in performance is attributed to an extension of the excitons dissociation area and to faster charge carrier transport through the nanotubes. No improvement in either V_{oc} or FF was observed. It is prudent to expect further improvement in FF by device optimization. These results indicate that the length of the CNT as a charge carrier is an important parameter to be considered in their implementation in OPV and possibly in other photonic devices.

AUTHOR INFORMATION

Corresponding Author

*E-mail: Somenath.Mitra@njit.edu. Tel.: +1 973 596 5611. Fax: +1 973 596 3586.

Notes

The authors declare no competing financial interest.

REFERENCES

(1) Powell, C.; Bender, T.; Lawryshyn, Y. *Sol. Energy* **2009**, *83*, 1977−1984.
(2) Kalowekamo, J.; Baker, E. *Sol. Energy* **2009**, *83*, 1224−1231.
(3) Yap, C. C.; Yahaya, M.; Salleh, M. M. *Sol. Energy* **2011**, *85*, 95−99.
(4) Pivrikas, A.; Neugebauer, H.; Sariciftci, N. S. *Sol. Energy* **2011**, *85*, 1226−1237.
(5) Deibel, C.; Dyakonov, V. *Rep. Prog. Phys.* **2010**, *73*, 096401.
(6) Dang, M. T.; Wantz, G.; Bejbouji, H.; Urien, M.; Dautel, O. J.; Vignau, L.; Hirsch, L. *Sol. Energy Mater. Sol. Cells* **2011**, *95*, 3408−3418.
(7) Kalita, G.; Masahiro, M.; Koichi, W.; Umeno, M. *Solid-State Electron.* **2010**, *54*, 447−451.
(8) Lau, X. C.; Desai, C.; Mitra, S. *Sol. Energy* **2013**, *91*, 204−211.
(9) Derbal-Habak, H.; Bergeret, C.; Cousseau, J.; Nunzi, J. M. *Sol. Energy Mater. Sol. Cells* **2011**, *95* (0), S53−S56.
(10) Guangyong, L.; Liming, L. *Nanotechnol. Mag., IEEE* **2011**, *5*, 18−24.
(11) Li, C.; Chen, Y.; Wang, Y.; Iqbal, Z.; Chhowalla, M.; Mitra, S. *J. Mater. Chem.* **2007**, *17*, 2406−2411.
(12) Ren, S.; Bernardi, M.; Lunt, R. R.; Bulovic, V.; Grossman, J. C.; Gradečak, S. *Nano Lett.* **2011**, *11*, 5316−5321.
(13) Pradhan, B.; Batabyal, S. K.; Pal, A. J. *Appl. Phys. Lett.* **2006**, *88*, 093106.
(14) Kymakis, E.; Amaratunga, G. A. J. *Appl. Phys. Lett.* **2002**, *80*, 112−114.
(15) Stylianakis, M.M.; Kymakis, E. *Appl. Phys. Lett.* **2012**, *100*, 093301.
(16) Stylianakis, M. M.; Mikroyannidis, J. A.; Kymakis, E. *Sol. Energy Mater. Sol. Cells* **2010**, *94*, 267−274.
(17) Liu, L.; Stanchina, W. E.; Li, G. *Appl. Phys. Lett.* **2009**, *94*, 233309.
(18) Lau, X. C.; Wang, Z.; Mitra, S. *Appl. Phys. Lett.* **2013**, *103*, 243108.
(19) Li, C.; Chen, Y.; Ntim, S. A.; Mitra, S. *Appl. Phys. Lett.* **2010**, *96*, 143303.
(20) Li, C.; Mitra, S. *Appl. Phys. Lett.* **2007**, *91*, 253112.
(21) Cataldo, S.; Salice, P.; Menna, E.; Pignataro, B. *Energy Environ. Sci.* **2012**, *5*, 5919−5940.
(22) Kalita, G.; Adhikari, S.; Aryal, H. R.; Umeno, M.; Afre, R.; Soga, T.; Sharon, M. *Appl. Phys. Lett.* **2008**, *92*, 123508.
(23) Ratier, B.; Nunzi, J.-M.; Aldissi, M.; Kraft, T. M.; Buncel, E. *Polym. Int.* **2012**, *61*, 342−354.
(24) Tezuka, N.; Umeyama, T.; Seki, S.; Matano, Y.; Nishi, M.; Hirao, K.; Imahori, H. *J. Phys. Chem. C* **2010**, *114*, 3235−3247.
(25) Nismy, N. A.; Jayawardena, K. D. G. I.; Adikaari, A. A. D. T.; Silva, S. R. P. *Adv. Mater.* **2011**, *23*, 3796−3800.
(26) Dabera, G. D. M. R.; Jayawardena, K. D. G. I.; Prabhath, M. R. R.; Yahya, I.; Tan, Y. Y.; Nismy, N. A.; Shiozawa, H.; Sauer, M.; Ruiz-Soria, G.; Ayala, P.; Stolojan, V.; Adikaari, A. A. D. T.; Jarowski, P. D.; Pichler, T.; Silva, S. R. P. *ACS Nano* **2012**, *7*, 556−565.
(27) Kymakis, E.; Kornilios, N.; Koudoumas, E. *J. Phys. D: Appl. Phys.* **2008**, *41*, 165110.
(28) Lu, L.; Xu, T.; Chen, W.; Lee, J. M.; Luo, Z.; Jung, I. H.; Park, H. I.; Kim, S. O.; Yu, L. *Nano Lett.* **2013**, *13*, 2365−2369.
(29) Wang, X. X.; Wang, J. N.; Su, L. F. *J. Power Sources* **2009**, *186*, 194−200.
(30) Deng, X.; Xiong, D.; Wang, H.; Chen, D.; Jiao, Z.; Zhang, H.; Wu, M. *Carbon* **2009**, *47*, 1608−1610.

(31) Cheng, X.; Zhong, J.; Meng, J.; Yang, M.; Jia, F.; Xu, Z.; Kong, H.; Xu, H. *J. Nanomater.* **2011**, 938491.
(32) Li, G.; Shrotriya, V.; Huang, J.; Yao, Y.; Moriarty, T.; Emery, K.; Yang, Y. *Nat Mater.* **2005**, *4*, 864−868.